FINITE ELEMENT ANALYSIS IN COMBUSTION PHENOMENA

T. J. CHUNG, Y. M. KIM AND J. L. SOHN

Department of Mechanical Engineering, The University of Alabama in Huntsville, Huntsville, AL 35899, U.S.A.

SUMMARY

This paper is concerned with the exposition of finite element applications to combustion problems. The subject of computational fluid dynamics, including combustion calculations, has long been dominated by finite differences. Recently, however, the finite element method has emerged as a potential candidate for computational modelling in fluid mechanics. It is well known that reactive fluids with combustion present additional complications because of disparity in reaction rates commonly referred to as 'stiff'. The present paper reviews basic questions arising from combustion problems in applications of finite element techniques to the solution of problems associated with chemical kinetics, diffusion, waves, convection, etc. Finally, an example of a hydrogen–oxygen reaction is presented for practical applications. Extension to the finite element modelling of turbulence, sprays, boundary layers, shock waves, etc. in combustion must await significant developments of numerical strategies associated with a more complete understanding of physical phenomena and chemical kinetics.

KEY WORDS Combustion Numerical Modelling Finite Elements Stiff Equations

INTRODUCTION

Combustion modelling is the numerical simulation of combustion phenomena.[1,2] It describes the chemical and physical evolution of a complex reactive flow system by numerically solving the governing time-dependent conservation equations for mass, momentum and energy.

In combustion systems, the strongly exothermic processes of fuel oxidation may give rise to localized reaction zones which propagate themselves into the unreacted material near them.[3] There are two distinct mechanisms of propagation: deflagration and detonation. Deflagrations travelling through the unburned material at subsonic velocities depend for their propagation on the activation of adjacent material to a reactive condition by diffusive transport processes. Detonations, on the other hand, propagate at supersonic velocities by virtue of gas dynamic (shock) compression and heating of adjacent material, the shock itself being sustained by the energy released from the combustion process. In both cases, the reaction zone propagates as a consequence of strong coupling between the combustion chemistry and the appropriate fluid mechanical process.

Solving the equations of conservation requires input data such as the species present, the chemical reactions that can occur, transport coefficients for viscosity, thermal conductivity, molecular diffusion and thermal diffusion, the equations of state for the various materials present, and a set of boundary, source and initial conditions. Thus, these equations contain, in principle, all the information we might want from the largest microscopic space scales down to the point

---

Based on an Invited Lecture.

where the fluid approximation itself breaks down. Flame, detonation, turbulence phenomena and all multi-dimensional effects may be included in the solutions of these equations. There are several restrictions imposed on our modelling by the capacity of the computer memory, storage and processing speeds available. Thus, the solutions we arrive at are restricted and depend on both the time and space regimes we can afford to study and the numerical methods we have available to resolve them.

Modelling combustion systems has its own particular problems because of the strong interaction between the energy released from chemical reactions and the dynamics of fluid motion. The release of chemical energy generates gradients in temperature, pressure and density. These gradients, in turn, influence the transport of mass, momentum and energy in the system. On a large scale, the gradients may generate vorticity or affect the diffusion of mass and energy. On a microscopic scale, they are the origin of the turbulence which drastically affects microscopic mixing and burning velocities. Properly describing the strong interplay between chemistry and fluid dynamics is the real challenge of modelling combustion.

Our goal in this paper is to show how finite element techniques may be applied in combustion modelling. The subject of computational fluid dynamics, including combustion calculations, has been dominated by finite differences. Only recently has the finite element method emerged as a potential candidate for computational modelling in fluid mechanics.[4-19] In the sequel, we shall begin with introductory information on finite element applications in simple problems involved in sources and sinks of chemical kinetics, diffusion, waves and convection. Finally, an example of the hydrogen–oxygen reaction will be discussed, comparing the results with other methods.

Combustion problems associated with turbulence[20,21] and sprays[22-24] represent important physical phenomena. The exposition of these topics, however, must await more extensive future research.

COMBUSTION MODELLING

Conservation equations

The basic equations to solve in combustion problems include time-dependent equations for the conservation for mass, momentum and energy. In general, bulk viscosity, radiant heat flux, pressure gradient diffusion and thermal gradient diffusion with Soret and Dufour effects are neglected. With these assumptions, the conservation of mass, momentum and energy leads to the following equations.

Conservation of mass for the mixture

$$\frac{\partial \rho}{\partial t} + \nabla \cdot (\rho \mathbf{v}) = 0. \tag{1}$$

Conservation of mass for species

$$\rho \frac{\partial Y_k}{\partial t} + \rho (\mathbf{v} \cdot \nabla) Y_k + \nabla \cdot (\rho Y_k \mathbf{V}_k) = \omega_k, \tag{2a}$$

for k species;

$$\rho \frac{\partial Y}{\partial t} + \rho (\mathbf{v} \cdot \nabla) Y - \rho \nabla \cdot (D \nabla Y) = \omega, \tag{2b}$$

for one species using Fick's law.

Conservation of momentum

$$\rho \frac{\partial \mathbf{v}}{\partial t} + \rho(\mathbf{v}\cdot\nabla)\mathbf{v} + \nabla P - \nu(\nabla^2\mathbf{v} + \tfrac{1}{3}\nabla(\nabla\cdot\mathbf{v})) - \rho\sum_{k=1}^{N} Y_k\mathbf{f}_k = 0. \tag{3}$$

Conservation of energy

$$\rho c_{\mathrm{p}}\frac{\partial T}{\partial t} + \rho c_{\mathrm{p}}(\mathbf{v}\cdot\nabla)T - \frac{\partial P}{\partial t} - (\mathbf{v}\cdot\nabla)P - P\nabla\cdot\mathbf{v} - \sigma_{ij}\frac{\partial v_j}{\partial x_i}$$

$$- k\nabla^2 T + \nabla\cdot\left(\rho\sum_{k=1}^{N} h_k Y_k\mathbf{V}_k\right) - \rho\sum_{k=1}^{N} Y_k\mathbf{f}_k\cdot\mathbf{V}_k = 0, \tag{4a}$$

for *k* species

$$\rho c_{\mathrm{p}}\frac{\partial T}{\partial t} + \rho c_{\mathrm{p}}(\mathbf{v}\cdot\nabla)T - \frac{\partial P}{\partial t} - (\mathbf{v}\cdot\nabla)P - P\nabla\cdot\mathbf{v} - \sigma_{ij}\frac{\partial v_j}{\partial x_i}$$

$$- \nabla\cdot(\rho c_p D T\,\nabla Y) - \nabla\cdot(\rho c_p D Le\,\nabla T) = -h^0\omega, \tag{4b}$$

using Fick's law for one species without body forces.

Equation of state

$$P = \rho R T \sum_{k=1}^{N} Y_k/W_k, \tag{5}$$

where Y_k, W_k, $\mathbf{V}_k$ and $\mathbf{f}_k$ are the mass concentration, molecular weight, diffusion velocity and body force of species *k*, respectively; *Le* is the Lewis number, h^0 is the standard heat of formation, *D* is the diffusivity, *R* is the universal gas constant and ω is the reaction rate. It is seen that the last term on the LHS of equation (4b) becomes $\nabla\cdot(k\,\nabla T)$ if the Lewis number is unity. In most of the combustion problems, the body force effect may be neglected.

The governing equations for reacting fluids differ from those for non-reacting fluids mainly in the form of continuity and energy equations. There are *N* species continuity equations in addition to the continuity equation for the mixture. Therefore, the variables to be solved are the mixture density ρ, the species mass concentrations $Y_k (k = 1, 2, \ldots, N)$, the velocity field $\mathbf{v}$ $(i = 1, 2, 3)$, the temperature *T* and the pressure *P*. The $N + 6$ equations consist of

1 overall mass continuity:	equation (1)
$N - 1$ species equations:	equation (2b)
1 equation relating all Y_k:	$Y_1 + Y_2 + \cdots + Y_N = 1$
3 momentum equations:	equation (3)
1 energy equation:	equation (4a) or (4b)
1 equation of state:	equation (5)

It is possible to solve the energy and species equations with the diffusion velocities as unknown variables. In this case, however, the following additional equations are required:

$$\nabla X_i = \sum_{j=1}^{N} \frac{X_i X_j}{D_{ij}}(\mathbf{V}_j - \mathbf{V}_i), \tag{6}$$

where the mole fraction X_i is given by

$$X_i = \frac{Y_i/W_i}{\displaystyle\sum_{j=1}^{N} (Y_j/W_j)}. \tag{7}$$

The specific problems to be modelled are determined by the initial conditions, the boundary conditions, the set of chemical constituents and their thermophysical and chemical properties. These conditions often determine the choice of solution techniques.

Problems in modelling reactive flows

In the previous section, several generic problems associated with the solution of equations (1)–(7) were described. These problems, which must be overcome in order to accurately model transient combustion systems, are associated with multiple time scales, multiple space scales, geometric complexity and physical complexity.

The first class of problems arises in characterizing ordinary flame and detonation by different time scales. These scales range over many orders of magnitude. When phenomena are modelled such that characteristic times of variation are shorter than the time step one can afford, the equations describing the phenomena are usually called 'stiff'. The equations describing many chemical reaction rates are stiff with respect to convection and diffusion. Two distinct modelling approaches—global implicit and time-split asymptotic—have been developed to solve the stiff equations.[25,26]

The second class of problems involves the disparity in space scales occurring in combustion problems. To model the steep gradients at a flame front, a grid spacing of 10^{-3} cm or smaller might be required. To model convection, grid spacings of 1 cm might be adequate. Complex phenomena such as turbulence, which occur on intermediate spatial scales, present a particular modelling problem.

The third set of obstacles arises because of the geometric complexity associated with real systems. Most of the detailed models developed to date have been one-dimensional. Thus, they give a very limited picture of how the energy release affects the hydrodynamics. Even though many processes in a combustion system can be modelled in one dimension, there are others, such as boundary layer growth or the formation of vortices and separating flows, which clearly require at least two-dimensional hydrodynamics.

The final set of obstacles to detailed modelling concerns physical complexity. Combustion systems usually have many interacting species. These are represented by sets of many coupled equations which must be solved simultaneously. Complicated ordinary differential equations describing the chemical reactions, or large matrices describing the molecular diffusion process, are costly and increase calculation time by orders of magnitude over idealized or empirical models.[27] The fundamental processes in combustion include chemical kinetics, laminar and turbulent hydrodynamics, thermal conductivity, viscosity, molecular diffusion, thermochemistry radiation, nucleation, surface effects, evaporation, condensation, etc. Before a model of a whole combustion system can be assembled, each individual process must be separately understood and modelled. These submodels are either incorporated into the larger detailed model directly or, if the time and space scales are too disparate, must be incorporated phenomenologically. For example, diffusion and thermal conductivity between a wall and the reacting gas can be studied separately and then incorporated directly into a detailed combustion model. Turbulence, however, can be modelled on its own space scales only in idealized cases. These more fundamental models must be used to develop phenomenological models for use in the microscopic detailed models. Resolution and computational cost prevent incorporating the detailed turbulence model directly.[20,21]

NUMERICAL MODELLING PRELIMINARIES

Here, we discuss the major problems encountered in numerically solving the different types of

terms occurring in equations (1)–(5). Since these equations are coupled and non-linear, the rigorous mathematical error estimates are not available. However, it is possible to evaluate many of the numerical difficulties which may arise from various sources as individually characterized below:

1. Chemical kinetics, source, and sink:

$$\frac{\partial c}{\partial t} = kc + d.$$

2. Diffusion and dissipative effects:

$$\frac{\partial u}{\partial t} = v\frac{\partial^2 u}{\partial x^2}.$$

3. Wave equations:

$$\frac{\partial^2 P}{\partial t^2} = a^2\frac{\partial^2 P}{\partial x^2}.$$

4. Convective or continuity equations:

$$\frac{\partial f}{\partial t} = -\frac{\partial}{\partial x}(fu).$$

Evaluations of each of the cases listed above will be discussed in the following subsections.

Chemical kinetics with source and sink

A number of local phenomena such as source terms, $d(x, t)$, and sink terms, $- k(x, t)c(x, t)$, may be given by

$$\frac{\partial c}{\partial t} = kc + d, \tag{8}$$

where, if c is a two-component vector containing a thermal and a vibrational temperature, terms such as $(kc + d)$ express temperature equilibration at the rate $- k$. If d were a vector of chemical reactants, equation (8) would look like the typical kinetic rate equation. If k and c are constant, this equation has the analytical solution

$$c(t) = \left(c(0) + \frac{d}{k}\right)e^{kt} - \frac{d}{k}. \tag{9}$$

The finite element analogue of equation (8) may be developed as follows: let c be approximated as

$$c = \Phi_\alpha C_\alpha \tag{10}$$

where Φ_α is the finite element trial function, with α being the global node. Applying the orthogonal projections of the residual of the differential equation on the subspace spanned by test functions in the spatial and temporal domain, we obtain

$$\int_0^1 \left[\int_0^l \left(\frac{\partial c}{\partial t} - kc - d\right)W_\alpha \, \mathrm{d}x\right]W \, \mathrm{d}\xi = 0. \tag{11}$$

Here, W_α is the spatial test function, W is the temporal test function and ξ is the dimensionless time:

$$\xi = t/\Delta t. \tag{12}$$

Choosing $W_\alpha = \Phi_\alpha$ (Galerkin approximation) and setting

$$C_\alpha(t) = (1 - \xi)C_\alpha^n + \xi C_\alpha^{n+1}, \tag{13}$$

the finite element equation takes the form

$$\int_0^1 \left\{ A_{\alpha\beta} \frac{C_\beta^{n+1} - C_\beta^n}{\Delta t} - kA_{\alpha\beta}[(1 - \xi)C_\beta^n + \xi C_\beta^{n+1}] - D_\alpha \right\} W \, d\xi = 0,$$

or

$$(1 - k\,\Delta t\,\theta)A_{\alpha\beta}C_\beta^{n+1} = [1 + k\,\Delta t(1 - \theta)]A_{\alpha\beta}C_\beta^n + D_\alpha, \tag{14}$$

where

$$A_{\alpha\beta} = \int_0^l \Phi_\alpha \Phi_\beta \, dx \qquad (\alpha, \beta = \text{global nodes}), \tag{15}$$

$$D_\alpha = \int_0^l d\Phi_\alpha \, dx \tag{16}$$

$$\theta = \int_0^1 \xi W \, d\xi \bigg/ \int_0^1 W \, d\xi \tag{17}$$

Solving equation (14) for C_α^{n+1} yields

$$C_\alpha^{n+1} = \eta C_\alpha^n + G_\alpha, \tag{18}$$

with

$$\eta = \frac{1 + k\,\Delta t(1 - \theta)}{1 - k\,\Delta t\,\theta}, \tag{19}$$

$$G_\alpha = [(1 - k\,\Delta t\,\theta)A_{\alpha\beta}]^{-1}D_\beta \tag{20}$$

Let the errros at the $(n + 1)$th step and the nth step be given by ε_α^{n+1} and ε_α^n, respectively. If these errors are added to equation (18), then

$$C_\alpha^{n+1} + \varepsilon_\alpha^{n+1} = \eta(C_\alpha^n + \varepsilon_\alpha^n) + G_\alpha. \tag{21}$$

Subtracting equation (18) from equation (21) gives

$$\varepsilon_\alpha^{n+1} = \eta\varepsilon_\alpha^n. \tag{22}$$

For stable solutions, we must assure that errors at the nth step do not grow at the $(n + 1)$th step, that is

$$|\varepsilon_\alpha^{n+1}| \leqslant |\varepsilon_\alpha^n|. \tag{23}$$

This requirement can be met if

$$\eta \leqslant 1. \tag{24}$$

In accordance with traditional definitions in the finite difference literature, the following classifications may be given for negative k:

$$\theta = 1, \quad \text{implicit scheme,} \tag{25a}$$

$$\theta = 0, \quad \text{explicit scheme;} \tag{25b}$$

$$\theta = \tfrac{1}{2}, \quad \text{centred scheme.} \tag{25c}$$

To compare the results obtained above with the finite difference approach, we proceed as follows: the exact solution to equation (8) takes the form

$$c(t) = \left(c(0) + \frac{d}{k} \right) e^{kt} - \frac{d}{k}, \tag{26}$$

whereas the finite difference analogue yields

$$\frac{C^{n+1} - C^n}{\Delta t} = k[(1 - \xi)C^n + \xi C^{n+1}] + d. \tag{27}$$

Equation (27) can be solved for C^{n+1}:

$$C^{n+1} = \frac{1 + k\,\Delta t(1 - \xi)}{1 - k\,\Delta t\,\xi} C^n + \frac{\Delta t}{1 - k\,\Delta t\,\xi} d, \tag{28}$$

or

$$C^{n+1} = EC^n + G, \tag{29}$$

where

$$E = \frac{1 + k\,\Delta t(1 - \xi)}{1 - k\,\Delta t\,\xi},$$

$$G = \frac{\Delta t}{1 - k\,\Delta t\,\xi} d.$$

It is interesting to note that equation (29) is quite similar to equation (18). An alternative form of the solution to equation (28) may be written as

$$C^{n+1} = E\left(c(0) + \frac{d}{k} \right) - \frac{d}{k}, \tag{30}$$

where E is considered to be a finite difference approximation to the exponential function appearing in equation (26). The best approximation to the exponential occurs when $\xi = 1/2$:

$$E = 1 + k\,\Delta t + \frac{(k\,\Delta t)^2}{2} + \frac{(k\,\Delta t)^3}{4} + \cdots, \tag{31}$$

which is correct up to the second order and has a third order error term $(k\,\Delta t)^3/12$.

With linear finite element trial and test functions for both the spatial and temporal domains, it would be clear that the results obtained in equations (27)–(31) can be reproduced. If higher order trial and test functions are chosen, then the formula given by (20) can be modified to provide highly sophisticated schemes both in spatial and temporal approximations.

The solutions for $k < 0$, $d = 0$ and $c(0) = 1$ using the linear finite element solutions are shown in Figure 1. It is seen that if $-k\,\Delta t$ is small, all of the numerical solutions are stable. For $-k\,\Delta t = 2$, however, the explicit scheme is violently unstable. This trend occurs when the equation is 'stiff', as characterized by

$$-\frac{kc}{dc/dt} \gg 1. \tag{32}$$

This situation also arises when the implicit parameter η or E becomes negative. The implicit scheme is unconditionally stable, but for large values of $-k\,\Delta t$, accuracy deteriorates rapidly, which is basically the same conclusion for standard finite difference schemes.
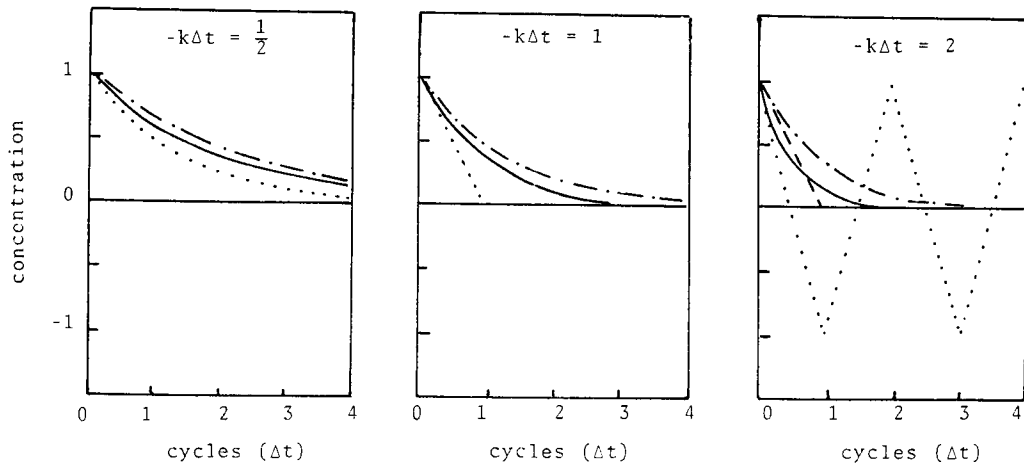
Figure 1. Comparisons of finite element solutions with analytical solutions for chemical kinetics (concentration vs. cycles): ..... explicit; ——— centred; —·— implicit; ——— analytical

Diffusion equations and dissipative effects

Consider a simple diffusion equation of the form

$$\frac{\partial u(x,t)}{\partial t} = v\frac{\partial^2 u(x,t)}{\partial x^2}.$$ (33)

The finite element equation corresponding to this is

$$\int_0^1 (A_{\alpha\beta}\dot{u}_\beta + B_{\alpha\beta}u_\beta)\overset{*}{W}\,\mathrm{d}\xi = 0,$$ (34)

or

$$(A_{\alpha\beta} + \theta\,\Delta t B_{\alpha\beta})u_\beta^{n+1} = [A_{\alpha\beta} - (1-\theta)\,\Delta t B_{\alpha\beta}]u_\beta^n,$$ (35)

where

$$B_{\alpha\beta} = \int_0^l \frac{\partial\Phi_\alpha}{\partial x}\frac{\partial\Phi_\beta}{\partial x}\,\mathrm{d}x.$$ (36)

Solving for u_α^{n+1} gives

$$u_\alpha^{n+1} = C_{\alpha\gamma}^{-1} D_{\gamma\beta} u_\beta^n$$ (37)

with

$$C_{\alpha\gamma} = A_{\alpha\gamma} + \theta\,\Delta t B_{\alpha\gamma},$$ (38)

$$D_{\gamma\beta} = A_{\gamma\beta} - (1-\theta)\,\Delta t B_{\gamma\beta}.$$ (39)

For an explicit scheme, $\theta = 0$, we have $C_{\alpha\gamma} = A_{\alpha\gamma}$ and $D_{\gamma\beta} = A_{\gamma\beta} - \Delta t B_{\gamma\beta}$. The errors at stations $n + 1$ and n are

$$\varepsilon_\alpha^{n+1} = g_{\alpha\beta}\varepsilon_\beta^n,$$ (40)

where $g_{\alpha\beta}$ is the amplification matrix

$$g_{\alpha\beta} = \delta_{\alpha\beta} - \Delta t A_{\alpha\gamma}^{-1} B_{\gamma\beta}.$$ (41)

To ensure stability, we must maintain

$$|g_{\alpha\beta}| \leqslant |\delta_{\alpha\beta}|.$$ (42)

In view of equations (39) and (40), and setting $\varepsilon_\alpha^{n+1} = \lambda\varepsilon_\alpha^n$, we write

$$(g_{\alpha\beta} - \lambda\delta_{\alpha\beta})\varepsilon_\beta^n = 0. \tag{43}$$

The stability of the solution to equation (37) can be assured if each and every eigenvalue λ_α of the amplification matrix (41) is made smaller than unity:

$$|\lambda_\alpha| \leqslant 1. \tag{44}$$

Obviously, the largest eigenvalue, called the spectral radius, governs the stability. Since there exists a bound for Δt outside of which stability can no longer be maintained, the explicit scheme here is said to be 'conditionally stable'. Note that Δt can be explicitly determined from equation (41) satisfying equation (44).

The amplification matrix for the implicit scheme, $\theta \neq 0$, is identified as

$$g_{\alpha\beta} = C_{\alpha\gamma}^{-1} D_{\gamma\beta}. \tag{45}$$

It is clear that Δt is implicit and cannot be determined explicitly. For a predetermined Δt, however, it is only possible to examine whether or not the stability criterion, equation (44), can be satisfied. The advantage of an implicit scheme is that, however large Δt is, the amplification matrix will always satisfy the requirement of equation (42), leading to an 'unconditionally stable' situation.

To provide discussions equivalent to the finite difference point of view, we may consider a finite element system consisting of two one-dimensional linear elements with global node numbers 1, 2 and 3 corresponding to the finite difference nodes $i - 1$, i and $i + 1$, respectively. The assembled matrix equations for $A_{\alpha\beta}$ and $B_{\alpha\beta}$ are

$$A_{\alpha\beta} = \sum_{e=1}^{E} A_{NM}^{(e)} \Delta_{N\alpha}^{(e)} \Delta_{M\beta}^{(e)} = \frac{\Delta x}{6} \begin{bmatrix} 2 & 1 & 0 \\ 1 & 4 & 1 \\ 0 & 1 & 2 \end{bmatrix},$$

$$B_{\alpha\beta} = \sum_{e=1}^{E} B_{NM}^{(e)} \Delta_{N\alpha}^{(e)} \Delta_{M\beta}^{(e)} = \frac{v}{\Delta x} \begin{bmatrix} 1 & -1 & 0 \\ -1 & 1 & -1 \\ 0 & -1 & 1 \end{bmatrix},$$

where N and M denote local nodes, $e = 1, \ldots, E$ refer to local elements, and $\Delta_{N\alpha}^{(e)}$ is the Boolean matrix for assembly. Expanding the second equation corresponding to the global node 2 or the finite difference node i, we obtain

$$\frac{2}{3\Delta t}(u_i^{n+1} - u_i^n) = \frac{v\theta}{\Delta x^2}[u_{i-1}^{n+1} - 2u_i^{n+1} - u_{i+1}^{n+1}] + \frac{v(1-\theta)}{\Delta x^2}[u_{i-1}^n - 2u_i^n + u_{i+1}^n]. \tag{46}$$

Notice that this is identical to the standard finite difference equation written at the node i except for the factor $1/3$ on the RHS.

If the spatial variation $e^{ik\Delta x}$ is assumed, where i is the complex unit, it can be shown that equation (46) takes the form

$$\frac{u^{n+1}(k) - u^n(k)}{\Delta t} = -\frac{3v\theta}{\Delta x^2}(1 - \cos k\,\Delta x)u^{n+1}(k) - \frac{3v(1-\theta)}{\Delta x^2}(1 - \cos k\,\Delta x)u^n(k), \tag{47}$$

from which the amplification factor may be calculated:

$$A(k) = \frac{u^{n+1}(k)}{u^n(k)} = \frac{1 - \dfrac{3v(1-\theta)\,\Delta t}{\Delta x^2}(1 - \cos k\,\Delta x)}{1 + \dfrac{3v\theta\,\Delta t}{\Delta x^2}(1 - \cos k\,\Delta x)}. \tag{48}$$
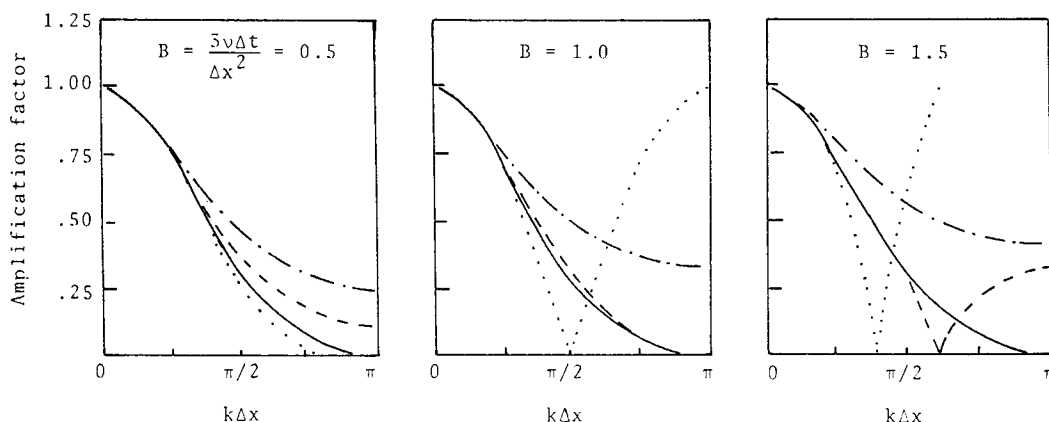
Figure 2. Comparisons of finite element solutions with analytical solutions for diffusion amplification factor: ..... explicit; — — — centred; — · — implicit; ——— analytical

This is seen to be the same form as equation (45) expanded into a two-element system.

The analytical solution to equation (33) in the time interval Δt decays by an amount

$$A(k) = \frac{u^{n+1}}{u^n} = e^{-vk^2\Delta t}. \tag{49}$$

To compare the numerical scheme with the analytical solution, we set

$$\mathbf{B} = \frac{3v\,\Delta t}{\Delta x^2}. \tag{50}$$

Thus, the analytical solution is recast as

$$A(k) = e^{-(1/3)(k\Delta x)^2}, \tag{51}$$

which is the $(1/B)$th root of equation (49) and expresses the amplification factor per unit time rather than per unit time step. Similarly, the finite element solution is written as

$$A(k) = \left[\frac{1 - B(1 - \theta)(1 - \cos k\,\Delta x)}{1 + B\theta(1 - \cos k\,\Delta x)} \right]. \tag{52}$$

Based on the results of these analyses, diffusion amplification factors are plotted in Figure 2. As expected, the implicit scheme is always stable, but it is not as accurate as the centred scheme for $B \leqslant 1\cdot0$. If B is increased to $1\cdot5$, both explicit and centred schemes are unstable. In general, for long wavelengths (small $k\,\Delta x$), all schemes are stable and accurate. If wavelengths are decreased, numerical difficulties are likely to occur. It is interesting to note that the results presented here are identical to those obtained by finite difference methods.

Wave equations

The propagation of waves is represented by

$$\frac{\partial^2 P}{\partial t^2} = a^2 \frac{\partial^2 P}{\partial x^2} \tag{53}$$

where, for example, a denotes the speed of sound in a material. The finite element analogue of

equation (53) now requires at least the quadratic temporal function for the time-dependent term. If the origin is placed at the centre of the temporal element, then

$$P_\alpha = \tfrac{1}{2}\xi(\xi - 1)P_\alpha^{n+1} + (1 - \xi^2)P_\alpha^n + \tfrac{1}{2}\xi(\xi + 1)P_\alpha^{n+1}$$

Therefore,

$$\frac{\partial^2 P}{\partial t^2} = \frac{\partial}{\partial t}\left(\frac{\partial P}{\partial t}\right) = \frac{\partial}{\partial \xi}\left(\frac{\partial P}{\partial t}\right)\frac{\partial \xi}{\partial t} = \frac{\partial^2 P}{\partial \xi^2}\left(\frac{\partial \xi}{\partial t}\right)^2$$

$$= \frac{1}{\Delta t^2}(P^{n-1} - 2P^n + P^{n+1}).$$

The global Galerkin finite element equation takes the form

$$\int_{-1}^{1}\left[\int_0^l \left(\frac{\partial^2 P}{\partial t^2} - a^2\frac{\partial^2 P}{\partial x^2}\right)\Phi_\alpha\,dx\right]W\,d\xi = 0, \tag{54}$$

or

$$(A_{\alpha\beta} + \eta\,\Delta t^2 B_{\alpha\beta})P_\beta^{n+1} = [2A_{\alpha\beta} - (\tfrac{1}{2} - 2\eta + \zeta)\,\Delta t^2 B_{\alpha\beta}]P_\beta^n$$
$$- [A_{\alpha\beta} + (\tfrac{1}{2} + \eta - \zeta)\,\Delta t^2 B_{\alpha\beta}]P_\beta^{n-1}, \tag{55}$$

where

$$\eta = \frac{\dfrac{1}{2}\displaystyle\int_{-1}^1 \xi(1 + \xi)\,W\,d\xi}{\displaystyle\int_{-1}^1 W\,d\xi}, \quad \zeta = \frac{\displaystyle\int_{-1}^1\left(\xi + \frac{1}{2}\right)W\,d\xi}{\displaystyle\int_{-1}^1 W\,d\xi}.$$

Once again, various choices are available for W. Some of the possibilities are shown below:

$$W = \delta(\xi + 1), \quad \eta = 0, \quad \zeta = \tfrac{1}{2};$$

$$W = \delta(\xi - 1), \quad \eta = 1, \quad \zeta = \tfrac{3}{2}, \text{ central explicit;}$$

$$W = 1 - \xi^2, \quad \eta = \tfrac{1}{10}, \quad \zeta = \tfrac{1}{2}, \text{ linear acceleration;}$$

$$W = \tfrac{1}{2}\xi(\xi + 1), \quad \eta = \tfrac{4}{5}, \quad \zeta = \tfrac{3}{2}, \text{ Galerkin.}$$

The stability analysis may be performed in a manner similar to that for the diffusion equation, but the histories of two time steps behind the current time step must be maintained.

The same physical phenomena depicted in equation (53) may be represented by two coupled first-order equations:

$$\frac{\partial P}{\partial t} = -a\frac{\partial Q}{\partial x}, \tag{56a}$$

$$\frac{\partial Q}{\partial t} = -a\frac{\partial P}{\partial x}. \tag{56b}$$

The global finite element equation corresponding to equation (56a) reads

$$\int_0^1\left[\int_0^l \left(\frac{\partial P}{\partial t} + a\frac{\partial Q}{\partial x}\right)\Phi_\alpha\,dx\right]W\,d\xi = 0, \tag{57}$$

or

$$\int_0^1 (A_{\alpha\beta}\dot{P}_\beta + E_{\alpha\beta}Q_\beta)W\,d\xi = 0. \tag{58a}$$

Similarly, equation (56b) takes the form

$$\int_0^1 (A_{\alpha\beta}\dot{Q}_\beta + E_{\alpha\beta}P_\beta)W\,\mathrm{d}\xi = 0. \tag{58b}$$

where

$$E_{\alpha\beta} = a \int_0^l \Phi_\alpha \frac{\partial \Phi_\beta}{\partial x}\,\mathrm{d}x = a \sum_{e=1}^E E_{NM}^{(e)} \Delta_{N\alpha}^{(e)} \Delta_{M\beta}^{(e)},$$

$$E_{NM}^{(e)} = a \int_0^{\Delta x} \Phi_N \frac{\partial \Phi_M}{\partial x}\,\mathrm{d}x = \frac{a}{2}\begin{bmatrix} -1 & 1 \\ -1 & 1 \end{bmatrix}.$$

Upon integration in the temporal domain, we arrive at

$$A_{\alpha\beta}P_\beta^{n+1} + \theta\,\Delta t E_{\alpha\beta}Q_\beta^{n+1} = A_{\alpha\beta}P_\beta^n - (1-\theta)\,\Delta t E_{\alpha\beta}Q_\beta^n. \tag{59a}$$

Similarly, from equation (56b), we obtain

$$A_{\alpha\beta}Q_\beta^{n+1} + \theta\,\Delta t E_{\alpha\beta}P_\beta^{n+1} = A_{\alpha\beta}Q_\beta^n - (1-\theta)\,\Delta t E_{\alpha\beta}P_\beta^n. \tag{59b}$$

The global finite element equation for equation (59a) written at node i as assembled from the two-element system reads

$$\frac{2}{3\,\Delta t}(P_i^{n+1} - P_i^n) = -\frac{a\theta}{2}[-Q_{i-1}^{n+1} + 2Q_i^{n+1} + Q_{i+1}^{n+1}]$$

$$-\frac{a(1-\theta)}{2}[-Q_{i-1}^n + 2Q_i^n + Q_{i+1}^{n+1}]. \tag{60a}$$

Likewise, from equation (60a),

$$\frac{1}{\Delta t}(Q_i^{n+1} - Q_i^n) = -\frac{3a\theta}{4\,\Delta x}[-P_{i-1}^{n+1} + 2P_i^{n+1} + P_{i+1}^{n+1}]$$

$$-\frac{3a(1-\theta)}{4\,\Delta x}[-P_{i-1}^n + 2P_i^n + P_{i+1}^n]. \tag{60b}$$

Wave equations have oscillatory solutions which we shall assume vary as

$$P(x,t) = P_k \mathrm{e}^{\mathrm{i}(kx - \omega t)}, \tag{61a}$$

$$Q(x,t) = Q_k \mathrm{e}^{\mathrm{i}(kx - \omega t)}, \tag{61b}$$

with

$$\omega = ak. \tag{62}$$

In terms of these representations, we may deduce from equation (60) the following numerical dispersion relation:

$$\sin\frac{\omega\,\Delta t}{2} = \alpha \sin\frac{k\,\Delta x}{2}, \quad \text{for the explicit scheme;} \tag{63}$$

$$\tan\frac{\omega\,\Delta t}{2} = \alpha \sin\frac{k\,\Delta x}{2}, \quad \text{for the implicit scheme;} \tag{64}$$
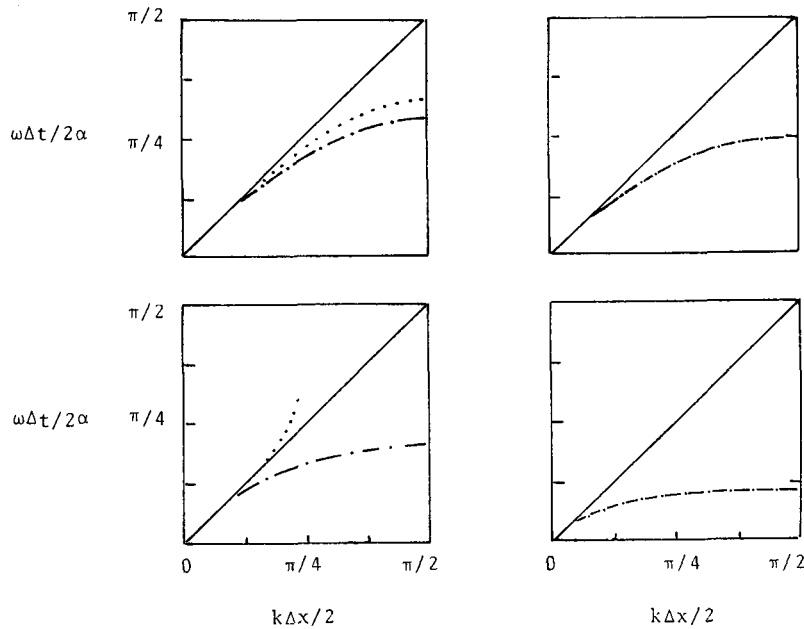
with

$$\alpha = \frac{a\,\Delta t}{\Delta x}. \tag{65}$$

Figure 3. Comparisons of finite element solutions with analytical solutions for dispersion relations of wave-like terms, $\alpha = a\,\Delta t/\Delta x$: ......explicit; —·— implicit; ——— analytical

These results are shown in Figure 3. For $\alpha = 1/2$, note that both explicit and implicit schemes behave closely together, whereas the explicit scheme agrees exactly with the analytical solution. The stability for the explicit scheme deteriorates rapidly for $\alpha > 1$. The implicit scheme is stable but rather inaccurate for short wavelengths. It is also seen that the explicit scheme is more accurate if stable. Once again, the conclusions here are the same as those obtained by finite difference methods.

Convective and continuity equations

The continuity equation,

$$\frac{\partial \rho(x,t)}{\partial t} = -\frac{\partial \rho(x,t)u(x,t)}{\partial x},$$ (66)

consists of convection and diffusion because the solution is sensitive to both phase and amplitude errors.

The finite element equation for equation (66) reads

$$\int_0^1 \left[\int_0^l \left(\frac{\partial \rho}{\partial t} + u\frac{\partial \rho}{\partial x} + \rho\frac{\partial u}{\partial x} \right)\Phi_\alpha \, dx \right] W\,d\xi = 0,$$ (67)

or

$$A_{\alpha\beta}\frac{\rho_\beta^{n+1} - \rho_\beta^n}{\Delta t} = -F_{\alpha\beta\gamma}[(1-\theta)(u_\beta\rho_\gamma)^n + \theta(\rho_\beta u_\gamma)^{n+1}],$$

where

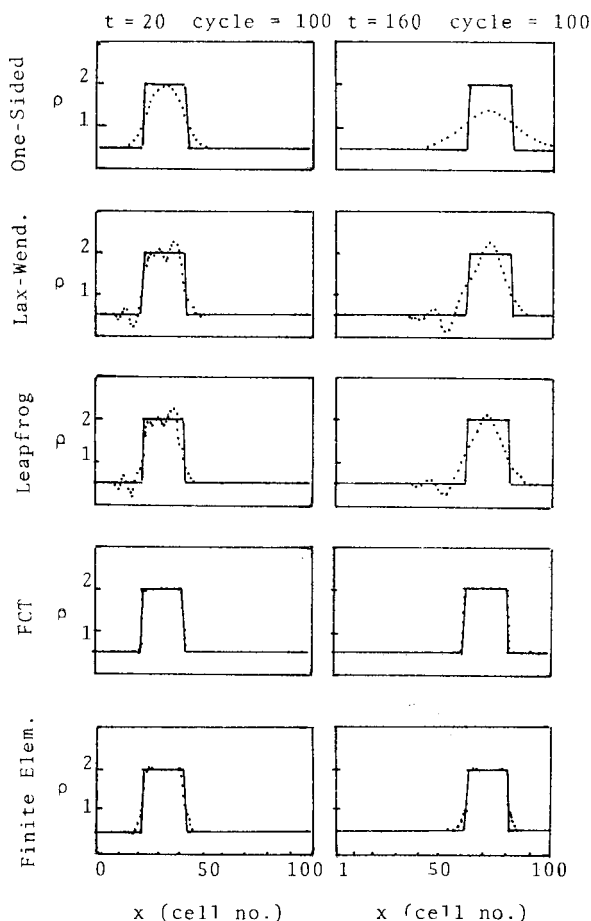$$F_{\alpha\beta\gamma} = \int_0^l \Phi_\alpha \Phi_\beta \frac{\partial \Phi_\gamma}{\partial x}\,dx.$$ (68)

Figure 4. Comparisons of finite element method (Taylor–Galerkin) with various finite difference schemes,[28] solution of one-dimensional square wave propagation, $\Delta t = 0.2$, $h = 1.0$, $u = 1.0$, Courant number $= 0.2$

It is seen that non-linearity may cause difficulty as well as the convection and diffusion if u is not constant. It u is constant, then the finite element equation is similar to equations (34) and (35).

Figure 4 shows the results of the constant velocity square wave propagation obtained using several of the traditional methods and the finite element method. As is evident in these results (one-sided donor-cell, Lax–Wendroff, leap-frog), the pronounced undershoots and overshoots are as serious as numerical diffusion. Note that a solution by the flux-corrected transport (FCT) algorithms employs strong low-order smoothing to remove Gibbs oscillations with much weaker second-order smoothing needed for numerical stability of the explicit integrations.[28,29]

To solve equation (67), in which u is assumed to be constant using finite elements, we make use of the Taylor–Galerkin method,[17] since the Galerkin finite element equation, (67), will, in general, be unstable. Expanding equation (66) in Taylor series in time:

$$\frac{\rho^{n+1} - \rho^n}{\Delta t} - \frac{\Delta t}{2}\frac{\partial^2 \rho^n}{\partial t^2} - \frac{\Delta t^2}{6}\frac{\partial^3 \rho^n}{\partial t^3} + u\frac{\partial \rho^n}{\partial x} = 0, \tag{69}$$

where

$$\frac{\partial^2 \rho^n}{\partial t^2} = u^2 \frac{\partial^2 \rho^n}{\partial x^2}, \tag{70}$$

$$\frac{\partial^3 \rho^n}{\partial t^3} = u^2 \frac{\partial^2}{\partial x^2}\left(\frac{\partial \rho^n}{\partial t}\right). \tag{71}$$

Rearranging equation (69),

$$\left(1 - \frac{u^2 \Delta t^2}{6}\frac{\partial^2}{\partial x^2}\right)\left(\frac{\rho^{n+1} - \rho^n}{\Delta t}\right) = -u\frac{\partial \rho^n}{\partial x} + \frac{u^2 \Delta t^2}{2}\frac{\partial^2 \rho^n}{\partial x^2}. \tag{72}$$

The Galerkin finite element equation for equation (72) yields

$$\int_\Omega \Phi_\alpha \left(1 - \frac{u^2 \Delta t^2}{6}\frac{\partial^2}{\partial x^2}\right)\left(\frac{\rho^{n+1} - \rho^n}{\Delta t}\right)\mathrm{d}\Omega = \int_\Omega \Phi_\alpha \left(-u\frac{\partial \rho^n}{\partial t} + \frac{u^2 \Delta t^2}{2}\frac{\partial^2 \rho^n}{\partial x^2}\right)\mathrm{d}\Omega. \tag{73}$$

The solution based on equation (73) in Figure 4 indicates that the finite element results are superior to those of donor-cell, Lax–Wendroff and leap-frog. It is expected that the FCT version of Taylor–Galerkin finite elements will further bring the results closer to the FCT finite differences.

Additional discussions of combustion modelling by finite elements will be given in the following section. Specifically, we shall consider a problem of the hydrogen–oxygen reaction using the Taylor–Galerkin finite element scheme with operator splitting.

TAYLOR–GALERKIN FINITE ELEMENT SCHEME WITH OPERATOR SPLITTING

General

One of the most efficient finite element schemes to handle stiff equations in combustion appears to be the Taylor–Galerkin finite elements with operator splitting.[17,30] The basic principle underlying this method begins by expanding the variables in terms of Taylor series. Let the governing equations be written in the form

$$\frac{\partial \mathbf{U}}{\partial t} + \frac{\partial F_j}{\partial x_j} - \frac{\partial G_j}{\partial x_j} = H, \tag{74}$$

with

$$\mathbf{U} = \begin{bmatrix} \rho \\ \rho u_i \\ \rho E \\ \rho Y_k \end{bmatrix}, \quad F_j = \begin{bmatrix} \rho u_j \\ \rho u_i u_j + P\delta_{ij} \\ u_j(\rho E + P) \\ \rho u_i Y_{ki} \end{bmatrix},$$

$$G_j = \begin{bmatrix} 0 \\ \sigma_{ij} \\ u_l\sigma_{ij} + k\dfrac{\partial T}{\partial x_j} \\ \rho D \dfrac{\partial Y_k}{\partial x_j} \end{bmatrix}, \quad \mathbf{H} = \begin{bmatrix} 0 \\ \rho \displaystyle\sum_{k=1}^{N} Y_k f_{ki} \\ \rho \displaystyle\sum_{k=1}^{N} Y_k f_{ki}(u_i + V_{ki}) \\ \omega_k \end{bmatrix},$$

$$\sigma_{ij} = \mu\left(\frac{\partial u_i}{\partial x_j} + \frac{\partial u_j}{\partial x_i}\right) + \lambda\frac{\partial u_k}{\partial x_k}\delta_{ij},$$

$$P = \rho R^0 T \sum_{k=1}^{N} \frac{Y_k}{W_k},$$

$$E = \sum_{k=1}^{N} h_k Y_k - \frac{P}{\rho} + \frac{u_i u_i}{2},$$

$$h_k = h_k^0 + \frac{T}{T_0} c_{pk} \, dT.$$

Expanding $\mathbf{U}$ in terms of Taylor series,

$$\mathbf{U}^{n+1} = \mathbf{U}^n + \Delta t \frac{\partial u^n}{\partial t} + \frac{\Delta t^2}{2} \frac{\partial^2 U^n}{\partial t^2} + O(\Delta t^3). \tag{75}$$

From equation (74) for the nth time-step

$$\frac{\partial \mathbf{U}^n}{\partial t} = -\frac{\partial F_j^n}{\partial x_j} + \frac{\partial G_j^n}{\partial x_j} + \mathbf{H}^n, \tag{76}$$

$$\frac{\partial^2 \mathbf{U}^n}{\partial t^2} = \frac{\partial}{\partial x_j} \left[\mathbf{A}_j \left(\frac{\partial \mathbf{F}_l^n}{\partial x_l} - \mathbf{H}^n \right) \right] + \mathbf{C} \left(\mathbf{H}^n - \frac{\partial \mathbf{F}_l^n}{\partial x_l} + \frac{\partial \mathbf{G}_l^n}{\partial x_l} \right), \tag{77}$$

where

$$\mathbf{A}_j = \frac{\partial \mathbf{F}_j^n}{\partial \mathbf{U}}, \quad \mathbf{C} = \frac{\partial \mathbf{H}^n}{\partial \mathbf{U}}.$$

Substituting equtions (76) and (77) into equation (75), we obtain

$$\mathbf{U}^{n+1} = \mathbf{U}^n - \Delta t \frac{\partial}{\partial x_j} \left[\mathbf{F}_j^n - \frac{\Delta t}{2} \mathbf{A}_j \left(\frac{\partial \mathbf{F}_l^n}{\partial x_l} - \mathbf{H}^n \right) \right]$$

$$+ \Delta t \left(\frac{\partial \mathbf{G}_j}{\partial x_j} + \mathbf{H}^n \right) + \frac{\Delta t^2}{2} \mathbf{C} \left(\mathbf{H}^n - \frac{\partial \mathbf{F}_l^n}{\partial x_l} + \frac{\partial \mathbf{G}_l^n}{\partial x_l} \right). \tag{78}$$

Now we split equation (78) into two steps:

Step 1

$$\mathbf{U}^{n+1/2} = \mathbf{U}^n - \frac{\Delta t}{2} \frac{\partial F_j^n}{\partial x_j}. \tag{79a}$$

Step 2

$$\mathbf{U}^{n+1} = \mathbf{U}^n + \Delta t \left(-\frac{\partial \mathbf{F}_j^{n+1/2}}{\partial x_j} + \frac{\partial \mathbf{G}_j^n}{\partial x_j} + \mathbf{H}^n \right) + \frac{\Delta t^2}{2} \mathbf{C} \left(-\frac{\partial \mathbf{F}_j^n}{\partial x_j} + \frac{\partial \mathbf{G}_j^n}{\partial x_j} + \mathbf{H}^n \right). \tag{79b}$$

Construct the Galerkin finite element equations from equation (79),

Step 1

$$\mathbf{U}_e^{n+1/2} = \int_{\Omega_e} \left(\Phi_\alpha U_\alpha^n - \frac{\Delta t}{2} \frac{\partial \Phi_\alpha}{\partial x_j} \mathbf{F}_{\alpha j}^n \right) d\Omega \Big/ \int_{\Omega_e} d\Omega_e \tag{80a}$$

Step 2

$$A_{\alpha\beta} \Delta U_\beta^{n+1} = F_\alpha^n \tag{80b}$$

where

$$A_{\alpha\beta} = \int_{\Omega} \Phi_{\alpha}\Phi_{\beta}\, d\Omega$$

$$F_{\alpha}^{n} = \Delta t \int_{\Gamma} \left(1 + \frac{\Delta t}{2}\mathbf{C}\right)(-\mathbf{F}_{j}^{n+1/2}n_{j} + \mathbf{G}_{j}^{n}n_{j})\Phi_{\alpha}\, d\Gamma$$

$$+ \Delta t \int_{\Omega} \frac{\partial \Phi_{\alpha}}{\partial x_{j}}\left(1 + \frac{\Delta t}{2}\mathbf{C}\right)(\mathbf{F}_{j}^{n+1/2} - \mathbf{G}_{j}^{n} + \mathbf{H}^{n})\, d\Omega$$

$$+ \frac{\Delta t^{2}}{2}\int_{\Omega} \Phi_{\alpha}\frac{\partial \mathbf{C}}{\partial x_{j}}(\mathbf{F}_{j}^{n+1/2} - \mathbf{G}_{j}^{n})\, d\Omega.$$

The above procedure is known as the two-step Taylor–Galerkin finite element method with computations to be carried out as follows:

1. Set up initial conditions at $t = 0$.
2. Compute derivative terms such as $\partial u_{j}/\partial x_{j}$, $\partial T/\partial x_{j}$ and $\partial Y_{k}/\partial x_{j}$.
3. Compute values at the $(n + 1/2)$th time-step in each element.
4. Compute values at the $(n + 1)$th time-step at each global node.
5. Repeat steps 2–4 until a steady state is reached.

In what follows, we shall demonstrate the above approach in the solution of hydrogen–oxygen reactions in one-dimensional laminar flow.

Hydrogen–oxygen system

Consider the quasi-one-dimensional chemically reacting supersonic flow of the premixed H_{2}–air system[31–33] as shown in Figure 5,

$$\frac{\partial \mathbf{U}}{\partial t} + \frac{\partial \mathbf{F}}{\partial x} = \mathbf{H}$$

with

$$\mathbf{U} = \begin{bmatrix} \rho A \\ \rho u A \\ \rho E A \\ \rho Y_{k} A \end{bmatrix}, \quad \mathbf{F} = \begin{bmatrix} \rho u A \\ \rho u^{2} A + PA \\ \rho u H A \\ \rho u Y_{k} A \end{bmatrix}, \quad \mathbf{H} = \begin{bmatrix} 0 \\ P\dfrac{\mathrm{d}A}{\mathrm{d}x} \\ 0 \\ \omega_{k} A \end{bmatrix}, \tag{81}$$

in which A is the cross-sectional area, E is the stagnation internal energy per unit mass, H is the stagnation enthalpy per unit mass and ω_{k} is the production of species k.

The chemical model is of the form[31]

$$H_{2} + O_{2} \underset{k_{b1}}{\overset{k_{f1}}{\rightleftarrows}} 2OH \tag{82a}$$

$$2OH + H_{2} \underset{k_{b2}}{\overset{k_{f2}}{\rightleftarrows}} 2H_{2}O \tag{82b}$$

where

$$k_{fi} = A_{i}(\phi)T^{N_{i}}\exp(-E_{i}/R^{0}T), \quad k_{bi} = f_{fi}/k,$$
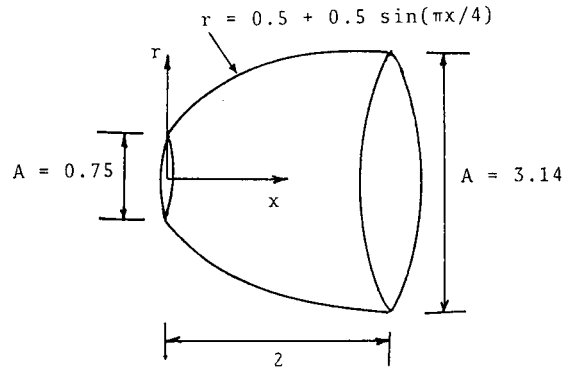
Figure 5. Rapid expansion supersonic diffuser. Inlet data: $M = 1\cdot4$, $u = 1230\,\text{m/s}$, $T = 1900\,\text{K}$, $P = 0\cdot081\,\text{MPa}$, $\phi = 0\cdot3$

$$A_1 = (8\cdot917 + 31\cdot433/\phi - 28\cdot950) \times 10^{47}\,(\text{cal/mole s}),$$

$$E_1 = 4865\,(\text{cal/mole}), \quad N_1 = -10,$$

$$A_2 = (2 + 1\cdot333/\phi - 0\cdot833) \times 10^{64}\,(\text{cal/mole s})$$

$$E_2 = 42{,}500\,(\text{cal/mole}), \quad N_2 = -13$$

and ϕ is the equivalence ratio. The rate of change of concentration of species j by reaction i becomes

$$\dot{C}_{j,i} = (v''_{ij} - v''_{ij})\left(k_{\text{f}i} \prod_{j=1}^{N_{\text{s}}} C_j^{v_{ij}} - k_{\text{b}i} \prod_{j=1}^{N_{\text{s}}} C_j^{v'_{ij}} \right), \tag{83}$$

with

$$\dot{C}_j = \sum_{i=1}^{N_{\text{R}}} C_{j,i}, \quad w_i = \dot{C}_j W_j, \quad \dot{C}_{\text{O}_2} = -k_{\text{f}1} C_{\text{H}_2} C_{\text{O}_2} + k_{\text{b}1} C_{\text{OH}}^2,$$

$$\dot{C}_{\text{H}_2\text{O}} = 2(k_{\text{f}2} C_{\text{OH}}^2 C_{\text{H}_2} - k_{\text{b}2} C_{\text{H}_2\text{O}}^2), \quad \dot{C}_{\text{H}_2} = \dot{C}_{\text{O}_2} - \tfrac{1}{2}\dot{C}_{\text{H}_2\text{O}},$$

$$\dot{C}_{\text{OH}} = -(2\dot{C}_{\text{O}_2} + \dot{C}_{\text{H}_2\text{O}}).$$

The thermodynamic model assumes the form

$$C_{\text{p}i} = a_i T + b_i, \quad \bar{c}_{\text{p}i} = \sum_{i=1}^{N_{\text{R}}} c_{\text{p}i} Y_i.$$

The total enthalpy of the mixture is

$$H = \sum_{i=1}^{N_{\text{R}}} \left[Y_i \int_0^T (c_{\text{p}i}\,\text{d}T + H_i^0) \right] + \frac{u^2}{2}$$

$$= \sum_{i=1}^{N_{\text{R}}} \left[Y_i \left(\frac{a_i}{2} T^2 + B_i T + H_i^0 \right) \right] + \frac{u^2}{2},$$

where h_i^0 is the reference enthalpy at $T = 0\,\text{K}$, and

$$\bar{R} = \sum_{i=1}^{N_{\text{R}}} R_i Y_i$$

is the mixture gas constant.

The operator splitting designed to maintain stability for stiffness equations is written as follows

$$\mathbf{U}^{n+1} = L_f L_c(\mathbf{U}^n), \tag{84}$$

where L_c is the chemistry operator

$$L_c(\mathbf{U}^n) = \frac{d\mathbf{U}^n}{dt} - \mathbf{H}^n = 0, \tag{85}$$

which is integrated by the 'stiff' implicit backward differentiation formulae, and L_f is the fluid operator

$$L_f(\mathbf{U}^{\tilde{n}}) = \frac{\partial \mathbf{U}^{\tilde{n}}}{\partial t} + \frac{\partial \mathbf{F}_j^{\tilde{n}}}{\partial x_j} - \frac{\partial \mathbf{G}_j^{\tilde{n}}}{\partial x_j} - \mathbf{H}^{\tilde{n}} = 0, \tag{86}$$

to be integrated by the explicit Taylor–Galerkin two-step scheme. Note that $\mathbf{U}^{\tilde{n}}$ is the solution of $L_c(\mathbf{U}^n) = 0$. The source terms $\mathbf{H}^{\tilde{n}}$ are zero for the species equation.

The Taylor–Galerkin two-step scheme for the fluid operator L_f gives rise to the following algorithm.

Step 1

$$\mathbf{U}^{n+1/2} = \mathbf{U}^{\tilde{n}} + \frac{\Delta t}{2} \left(\frac{\partial \mathbf{F}_j^{\tilde{n}}}{\partial x^j} + \mathbf{H}_j^{\tilde{n}} \right). \tag{87}$$

Step 2

$$\mathbf{U}^{n+1} = \mathbf{U}^{\tilde{n}} + \Delta t \left(\frac{\partial \mathbf{F}_j^{n+1/2}}{\partial x_j} + \frac{\partial \mathbf{G}_j^{n+1}}{\partial x_j} + \mathbf{H}_j^{n+1/2} \right), \tag{88}$$

where the source terms for species equations are zero.

Let Ψ_l be the piecewise trial function associated with node l and Φ_e be the piecewise constant trial function associated with element e, then

$$\mathbf{U}^n = \sum_l \mathbf{U}_l^n \Psi_l, \quad \mathbf{F}_j^n = \sum_l \mathbf{F}_{jl}^n \Psi_l, \quad \mathbf{U}^{n+1/2} = \sum_e U_e^{n+1/2} \Phi_e.$$

Constructing the weighted residual, we have[12]

$$\sum_e \left(\int_\Omega \Phi_E \Phi_e \, d\Omega \right) U_e^{n+1/2} = \sum_l \left(\int_\Omega \Phi_E \Phi_l \, d\Omega \right) U_l^{\tilde{n}} - \frac{1}{2} \Delta t \sum_l \left(\int_\Omega \Phi_E \frac{\partial \Psi_l}{\partial x_j} \, d\Omega \right) \mathbf{F}_{jl}^{\tilde{n}}$$
$$+ \frac{1}{2} \Delta t \sum_l \left(\int_\Omega \Phi_E \Psi_l \, d\Omega \right) \mathbf{H}_l^{\tilde{n}}, \tag{89}$$

where Φ_E assumes the value of one within the element E and zero elsewhere:

$$\int_\Omega \Phi_E \Phi_e \, d\Omega = A\delta_{Ee},$$

with δ_{Ee} being the Kronecker delta and A the area. Thus,

$$A\mathbf{U}_E^{n+1/2} = \sum_l \left(\int_{\Omega_E} \Psi_l \, d\Omega \right) \mathbf{U}_l^{\tilde{n}} - \frac{1}{2} \Delta t \sum_l \left(\int_{\Omega_E} \frac{\partial \Psi_l}{\partial x_j} \, d\Omega \right) \mathbf{F}_{jl}^{\tilde{n}}. \tag{90}$$

This concludes step 1. We then proceed to step 2:

$$\mathbf{U}^{n+1} = \mathbf{U}^n + \Delta t \left(\frac{\partial \mathbf{F}_j^{n+1/2}}{\partial x_j} + \frac{\partial \mathbf{G}_j^{n+1/2}}{\partial x_j} + \mathbf{H}_j^{n+1/2} \right), \tag{91}$$

where $\mathbf{H}^{n+1/2}$ is zero for species equations. The Galerkin finite element equations take the form

$$\mathbf{U}^{n+1/2} = \sum_l \mathbf{U}_l^{n+1}\Psi_l, \quad \mathbf{F}_j^{n+1/2} = \sum_e \mathbf{F}_j^{n+1/2}\Phi_e,$$

$$\mathbf{H}^{n+1/2} = \sum_e \mathbf{H}_l^{n+1/2}\Phi_e, \quad \mathbf{G}_j^n = \sum_l \mathbf{G}_{jl}^n\Psi_l,$$

$$\sum_l\left(\int_\Omega \Psi_m\Psi_l\,\mathrm{d}\Omega\right)(\mathbf{U}_l^{n+1/2} - \mathbf{U}_l^n) = \Delta t\sum_e\left(\int_\Omega \frac{\partial\Psi_m}{\partial x_j}\Phi_e\,\mathrm{d}\Omega\right)\mathbf{F}_{je}^{n+1/2}$$

$$-\Delta t\sum_e\left(\int_\Gamma n_j\Psi_m\Phi_e\,\mathrm{d}\Gamma\right)\mathbf{F}_{je}^{n+1/2}$$

$$-\Delta t\sum_e\left(\int_\Omega \frac{\partial\Psi_m}{\partial x_j}\Psi_e\,\mathrm{d}\Omega\right)\mathbf{G}_{je}^{n+1/2}$$

$$+\Delta t\sum_e\left(\int_\Gamma n_j\Psi_m\Psi_e\,\mathrm{d}\Gamma\right)\mathbf{G}_{je}^{n+1/2}$$

$$+\Delta t\sum_e\left(\int_\Omega \Psi_m\Phi_e\,\mathrm{d}\Omega\right)\mathbf{H}_e^{n+1/2}, \tag{92}$$

where n_j is the component of a vector normal to the surface.

Solutions are obtained through operations as described by steps 1 and 2 above, based on initial conditions at the inlet shown in Figure 5.[31] The initial conditions are assumed to be isentropic. Inlet boundary conditions are held constant at their initial values. Note that a rapid expansion diffuser is chosen so that high mass fraction gradients exist near the inlet.

In Figure 6, the time history of a hydrogen mass fraction at the first nodal point ($x = 0.02$) is shown. Here, the time discretization error tolerance is set at 10^{-8}. The time history of mass fractions shows two characteristic time scales: one associated with the formation of hydroxyl ($\simeq 10^{-11}$ s), another associated with the production of water ($\simeq 10^{-5}$ s). Agreement between the finite element solution and the spectral finite difference method is reasonably good. A similar trend is observed for oxygen, as shown in Figure 7. Figure 8 demonstrates the production of hydroxyl and water. Axial velocity profiles for $t = 0.1$ s, iteration number 2500, are shown in Figure 9. Here again, the finite element solution agrees well with the spectral finite difference
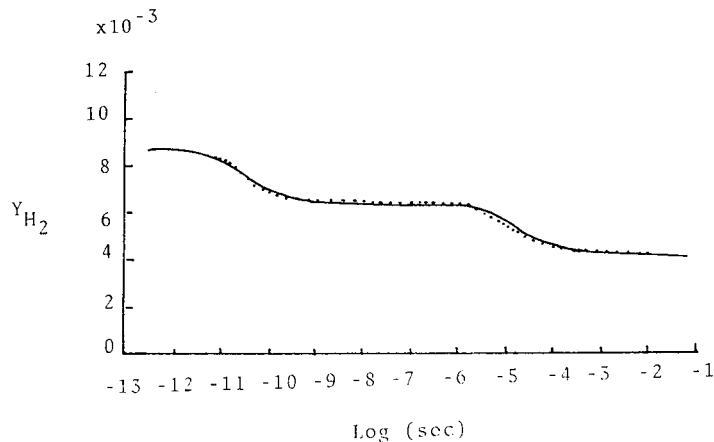

Figure 6. Time history of hydrogen mass fraction:———finite element method; ..... spectral method
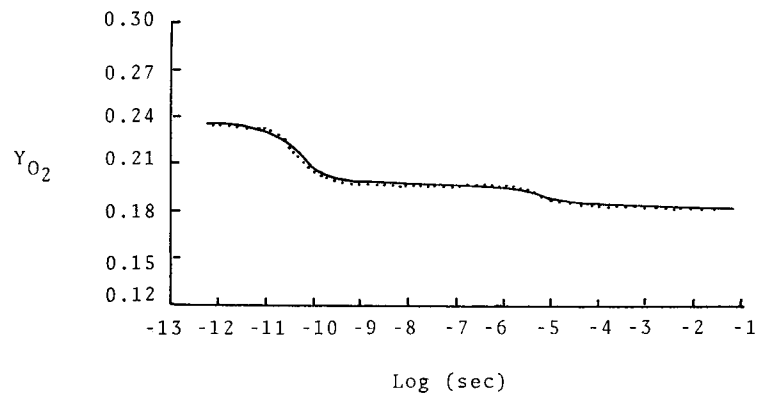
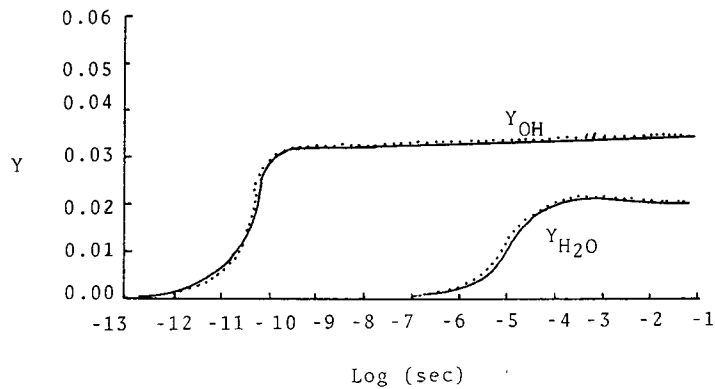Figure 7. Time history of oxygen mass fraction:——— finite element method;..... spectral method

Figure 8. Time history of hydrogen and water mass fraction:——— finite element method;..... spectral method
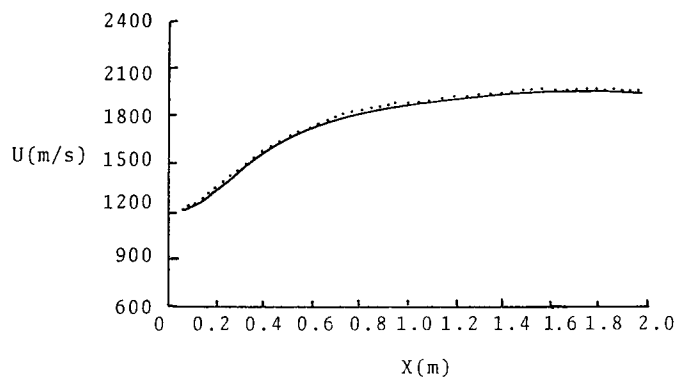
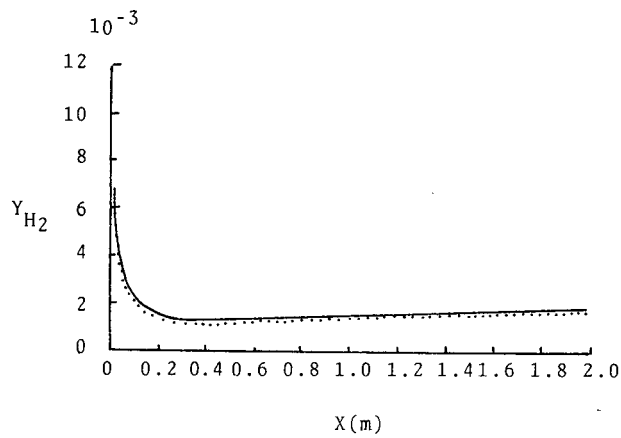Figure 9. Axial velocity profile:——— finite element method;..... spectral method

Figure 10. Axial hydrogen mass fraction profile: ———— finite element method; ..... spectral method
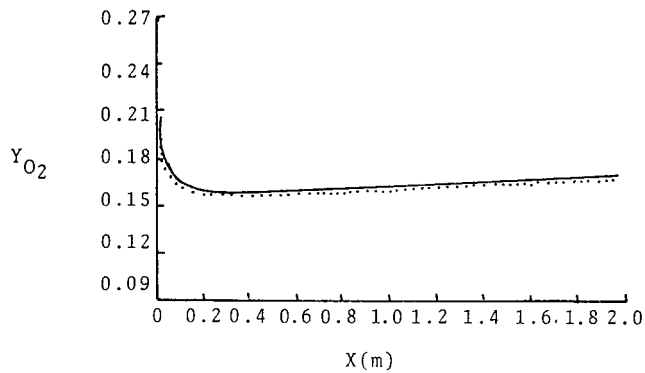

Figure 11. Axial oxygen mass fraction profile: ———— finite element method; ..... spectral method
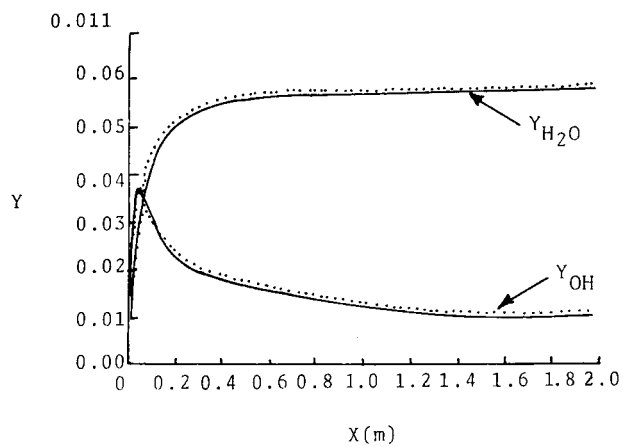

Figure 12. Axial hydroxyl and water mass fraction profiles: ———— finite element method; ..... spectral method

method.[31] The profiles of axial hydrogen, oxygen, hydroxyl and water mass fractions are depicted in Figures 10, 11 and 12, respectively, agreeing reasonably well with the spectral finite differences.

CONCLUSIONS

The finite element methods has emerged as a potential candidate for computational fluid dynamics[1-19] and, subsequently, for reactive fluids and combustion modelling. Introductory expositions on sources and sinks for chemical kinetics, diffusion, waves and convection, as well as an example of the hydrogen–oxygen reaction have been presented. In all of these examples, the results are compared with those of finite differences, indicating that both methods yield basically the same information in simple problems. For stiff equations, Taylor–Galerkin finite elements with operator splitting techniques appear to be stable and accurate.

Applications of finite elements to turbulence, sprays, boundary layers, shock waves, etc. in combustion problems must await extensive research in the future. Finite element applications dealing with non-linear, convective, stiff equations in combustion remain a great challenge in years to come.

REFERENCES

1. H. McDonald, 'Combustion modeling in two and three dimensions—some numerical considerations', *Progress in Energy and Combustion Science*, **5**, 97–122 (1979).
2. E. S. Oran and J. P. Boris, 'Detailed modeling of combustion systems', *Progress in Energy and Combustion Science*, **7**, 1–72 (1981).
3. F. A. Williams, *Combustion Theory*, Benjamin/Cummings Publishing Co., 1985.
4. T. J. Chung, *Finite Element Analysis in Fluid Dynamics*, McGraw-Hill Book Co., New York, 1978.
5. J. T. Oden and G. F. Carey, *Finite Elements: Mathematical Aspects*, Prentice Hall, Englewood Cliffs, 1981.
6. G. F. Carey and J. T. Oden, *Finite Elements: Fluid Mechanics*, Prentice Hall, Englewood Cliffs, 1981.
7. O. C. Zienkiewicz, R. Lohner and K. Morgan, 'High speed inviscid compressible flow by the finite element method', in J. R. Whiteman (ed.), *The Mathematics of Finite Elements and Applications*, V-MAFELAP, 1984, Academic Press, Ltd., London, 1985.
8. R. Glowinsky, Q. V. Dinh and J. Periaux, 'Domain decomposition methods for nonlinear problems in fluid dynamics', *Computer Methods in Applied Mechanics and Engineering*, **40**, 47–109 (1983).
9. T. J. R. Hughes, L. Franca and M. Mallet, 'A new finite element formulation for computational fluid dynamics: I. Symmetric forms of the compressible Euler and Navier–Stokes equation and the second law of thermodynamics', *Computer Methods in Applied Mechanics and Engineering*, **54**, 223–234 (1986).
10. T. J. R. Hughes, M. Mallet and A. Mizukami, 'A new finite formulation for computational fluid dynamics: II. Beyond SUPG', *Computer Methods in Applied Mechanics and Engineering*, **54**, 341–355 (1986).
11. R. Lohner, K. Morgan and L. Kong, 'An unstructured multigrid method for the compressible Euler equations', in D. Rues and W. Kordulla (eds.), *Proceedings, 6th GAMM Conference on Numerical Methods in Fluid Mechanics*, Vieweg Notes on Numerical Fluid Mechanics, Vol. 10, Vieweg Verlag, 1986.
12. R. Lohner, K. Morgan and O. C. Zienkiewicz, 'An adaptive finite element procedure for high speed flows', *Computer Methods in Applied Mechanics and Engineering*, **51**, 441–465 (1985).
13. T. J. Chung and J. L. Sohn, 'Interactions of coupled acoustic and vortical instability', *AIAA Journal*, **24**(10), 1582–1596 (1986).
14. T. Strouboulis, P. Devloo and J. T. Oden, 'A moving grid finite element algorithm for supersonic flow interaction between moving bodies', *Proceedings, 6th International Symposium on Finite Elements in Fluid Flows*, Antibes, France, June, 1986.
15. M. Bieterman and I. Babuska, 'An adaptive method of lines with error control for parabolic equations of the reaction–diffusion type', *Journal of Computational Physics*, **63**, 33–66 (1986).
16. J. T. Oden, P. Devloo and T. Strouboulis, 'Adaptive finite element methods for the analysis of inviscid compressible flow', *Proceedings, 6th International Symposium on Finite Elements in Fluid Flow*, June 1986.
17. J. Donea, S. Giuliani and H. Laval, 'Time-accurate solution of advection–diffusion problems by finite elements', *Computer Methods in Applied Mechanics and Engineering*, **45**, 123–145 (1984).
18. D. N. Lee and J. I. Ramos, 'Application of the finite element method to one-dimensional flame propagation problems', *AIAA Journal*, **21**, 262–269 (1983).
19. J. I. Ramos, 'The application of finite difference and finite element methods to a reaction–diffusion system in combustion', in C. Taylor, J. A. Johnson and W. R. Smith (eds), *Numerical Methods in Laminar and Turbulent Flow*, Pineridge Press, Swansea, UK, 1983, pp. 1137–1147.

20. P. A. Libby and F. A. Williams (eds), *Turbulent Reacting Flows*, Springer-Verlag, 1980.
21. W. P. Jones and J. H. Whitelaw, 'Modeling and measurements in turbulent combustion', *Proceedings, 20th International Symposium on Combustion*, 1984, 233–249.
22. W. A. Sirignano, 'The formulation of spray combustion models: resolution compared to droplet spacing', *Journal of Heat Transfer*, **108,** 633–639 (1986).
23. H. C. Gupta and F. V. Bracco, 'Numerical computations of two-dimensional unsteady sprays for applications to engines', *AIAA Journal*, **16**(10), 1053–1061 (1978).
24. W. A. Sirignano, 'Fuel droplet vaporization and spray combustion theory', *Progress in Energy and Combustion Science*, **9,** 291–322 (1983).
25. L. F. Shampine and C. W. Gear, 'A user's view of solving stiff ordinary differential equations', *SIAM Review*, **21**(1) 1–17 (1979).
26. R. J. Kee and H. A. Dwyer, 'Review of stiffness and implicit finite difference methods in combustion modeling', *Proceedings, 7th ICOGER*, Göttinger, FRG, 20–24, August 1979.
27. W. C. Gardiner, (ed.), *Combustion Chemistry*, Springer-Verlag, 1984.
28. J. P. Boris and D. L. Book, 'Flux-corrected transport. I. SHASTA, a fluid transport algorithm that works', *Journal of Computational Physics*, **11,** 38–69 (1973).
29. S. T. Zalesak, 'Fully multi-dimensional flux-corrected transport algorithms for fluids', *Journal of Computational Physics*, **31,** 335–362 (1979).
30. N. N. Yanenko, *The Method of Fractional Steps*, Springer-Verlag, New York, 1971.
31. J. P. Drummond and M. Y. Hussaini, 'Spectral methods for modeling supersonic chemically reacting flow fields', *AIAA paper, 85-0302*, January 1985.
32. J. S. Evans and C. J. Schexnayder, Jr., 'Influence of chemical kinetics and unmixedness on burning in supersonic hydrogen flames', *AIAA Journal*, **18**(2), 188–193 (1980).
33. T. R. A. Bussing and E. M. Murman, 'A finite volume method for the calculation of compressible chemically reacting flows', *AIAA Paper, 85-0331*, January 1985.